LOCAL DEFECT FORMATION IN SHORT GLASS FIBRE REINFORCED POLYMERS – MICRO-MECHANICAL SIMULATIONS AND INTERRUPTED IN-SITU EXPERIMENTS

Julia Maurer[a,b,*], Denise Krölling[b], Dietmar Salaberger[c], Michael Jerabek[c], Johann Kastner[a], Zoltán Major[b]

[a] *University of Applied Sciences Upper Austria, Research Group Computed Tomography, Stelzhamerstraße 23, 4600 Wels, Austria*

[b] *Johannes Kepler University Linz, Institute of Polymer Product Engineering, Altenberger Straße 69, 4040 Linz, Austria*

[c] *Borealis Polyolefine GmbH, St. Peter-Strasse 25, 4021 Linz, Austria*

[*] corresponding author: `julia.maurer@fh-wels.at`

Abstract. Discontinuous fibre reinforced polymers are widely used in various industry sectors and often replace conventional materials, due to lower production costs and their lightweight structure. For improvement of the component design, detailed knowledge of the failure mechanisms are necessary. To better understand the defect formation and thus the micro-mechanics, the strain behaviour in single fibres was analysed by micro-mechanical simulations of Representative Volume Elements (RVE). Therefore, selected fibres – similar orientated as in the real structure – were chosen for detailed analysis. Additionally, the defect formation next to selected fibres was investigated by X-ray computed tomography (CT). Furthermore, the critical fibre length was estimated based on the protruding fibre length of the fracture surface. Overall the simulation results correspond to theory. However, the detailed local inspection of the experimental volume data showed a rather strong influence of neighbouring fibres.

Keywords: Short fibre reinforced polymer, X-ray computed tomography, digital volume correlation, micro-mechanical simulation.

1. Introduction

Short glass fibre reinforced thermoplastics are a sub-category of composites. Parts and structures of complex shape can be produced in an automated fashion. Therefore, the main advantages are low manufacturing costs and the possibility of high-volume production. To improve these materials, detailed knowledge of the mechanical behaviour, especially at the micro-scale level, is of great importance.

X-ray computed tomography (CT) is a suitable method for the investigation of such materials and the ongoing damage processes [1]. For the analysis of the defect mechanisms and the quantification of the local strain distribution, interrupted in situ tensile tests are decisive [2, 3]. A rather new approach is the local strain evaluation based on Digital Volume Correlation (DVC), introduced 1999 by Bay et al. [4]. DVC enables the determination of the local displacements and further the calculation of local strains in three dimensions. For the correlation of the reference volume (unloaded state) and the deformed volume (loaded state), the fibres act as speckle pattern. Recent research on fibre reinforced materials using DVC has shown that the composite architecture contributes to sample failure at the mesoscale [5–7].

There are various modelling and simulation approaches of composites ranging from manufacturing process simulations to macro- and micro-scale simulations. The micro-structural details required for simulations are often provided by X-ray computed tomography data. In general, the mechanical behaviour of a fibre reinforced polymer is strongly influenced by the bonding between matrix and fibre. The deformation within the matrix is transmitted to the fibre by shear stresses between fibre and matrix interface. It is quantified by the so called interfacial shear strength or the critical fibre length [8]. There are various methods for a quantitative measurement of these values, further some models were developed in recent years. One of those is the Kelly-Tyson model [9].

The objective of this work was to determine local strain and defect formation, for a better understanding of the failure mechanisms of short glass fibre reinforced polymers at the micro-scale level. Additionally, the usage of the characterization of individual protruding fibres ("free fibres") for the estimation of interfacial shear strength based on the Kelly-Tyson model is presented.

2. Materials and methods

The investigated material is Polypropylene (PP) reinforced with $24\,wt\%$ of short glass fibres with a nominal fibre diameter of $13\,\mu m$. The mean and weighted mean fibre lengths are approx. $450\,\mu m$, respectively $810\,\mu m$,
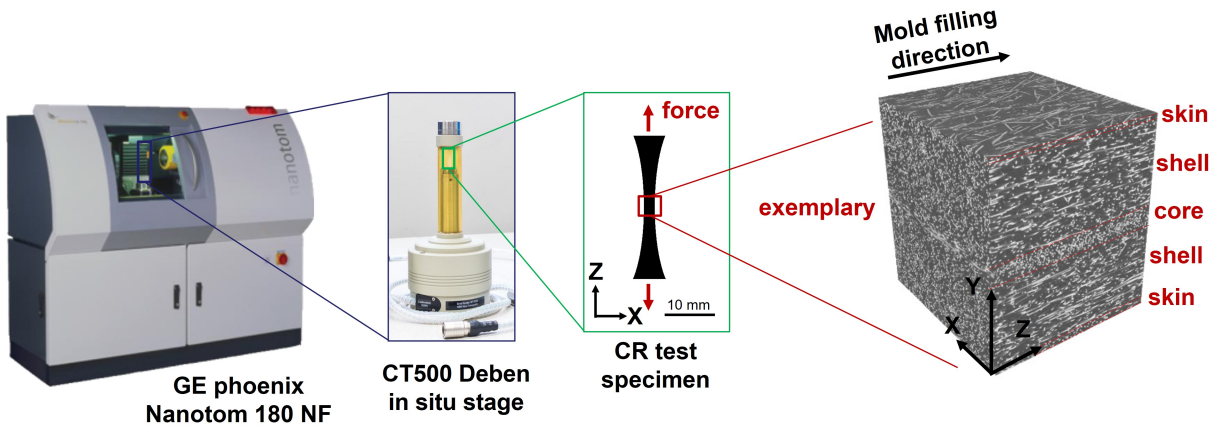
FIGURE 1. Experimental Setup for interrupted in situ CT measurements and exemplary CT volume (right), showing the typical skin-shell-core structure.

and were determined based on CT data.

A constant radius test geometry with a radius of 60 mm, a length of 30 mm and a narrowest cross section of 3×2 mm^2 was used for the tensile tests (see Figure 1). The CR test specimens were milled out from an injection moulded plate oriented in injection moulding direction. Thus resulting in a main fibre direction of 0°. Due to the injection moulding process the test specimens show a typical layered core-shell-skin structure, as well as transition regions in-between.

The constant radius test specimen (CR) was in situ tested in an interrupted manner until fracture similar as presented in [3]. The load steps were defined starting at 30 % of the tensile strength, followed by 52 % and then increased by 8 % until fracture. After each load step and a certain time until the sample was in a stable state, a CT scan was performed with the Nanotom 180NF device (phoenix|X-ray, GE Sensing & Inspection Technologies GmbH, Wunstorf, Germany) at a voxel edge length of 2 μm. The X-ray source was equipped with a tungsten-on-diamond target and operated at a voltage of 80 kV. The available analysis volume is approximately $3 \times 2 \times 3.6$ mm^3.

The local fibre characteristics were determined with the in house developed fibre characterization tool [10, 11]. This was done for the unloaded state to get the fibre length and orientation, and for the fractured surface to get the fibre length and orientation of the protruding fibres. For the latter some additional segmentation steps were necessary. First, a Gauss filter with kernel 5 was applied to the volume data to reduce the noise and facilitate the surface determination. Afterwards a surface determination with a gray value according to the material peak was applied and an region of interest (ROI) of the fracture surface with the protruded fibres was extracted. Some smoothing and open/close steps were followed by an inversion of the ROI, to be able to extract the protruded fibres only. Subsequent analysis of the ROI with the fibre characterization tool was performed.

The critical fibre length is a very important material

parameter for such materials. The critical fibre length is the minimum length to enable the fibre to contribute its full strength to the composite. Based on the Kelly-Tyson model the critical fibre length can be estimated with Equation (1) [9].

$$l_c = \frac{\sigma_{fibre} * d}{2 * \tau_{matrix}},\qquad(1)$$

whereas σ_{fibre} is the fibre strength and τ_{matrix} the interfacial shear strength. As the critical length is a function of the interfacial shear strength, it will influence the defect behavior (whether a fibre pull-out or fibre fracture occurs). Unfortunately, the interfacial shear strength is unknown. So the critical fibre length was estimated by evaluating the free fibres of the fracture surface from the CT data by conducting several segmentation steps. It was assumed, that the fibres were pulled out of both parts to the same extent. The critical length can than be estimated by selecting the longest pulled out fibres. It was decided to evaluate the length of the longest 10 fibres oriented in direction of the applied force.

For estimation of the local strain distribution inside the material the Avizo Software 3D (Thermo Fisher Scientific) and its Digital Volume Correlation (DVC) tool was used. A tetrahedral mesh with a average edge length of approximately 200 μm was used.

The Digimat software was used for the micromechanical simulations of representative volume elements (RVEs). The necessary work steps are shown in Figure 2. Generally, before starting simulations of representative volume elements, the material response needs to be known. A material model was derived by reverse engineering, based on mechanical experimental results (stress-strain curves of tested samples with main fibre orientation of 0°, 45° and 90°) and the knowledge of the fibre characteristics (fibre length, fibre orientation, fibre diameter) of these tested specimens. Initially, a suitable material model was used, which was iteratively adjusted by optimizing
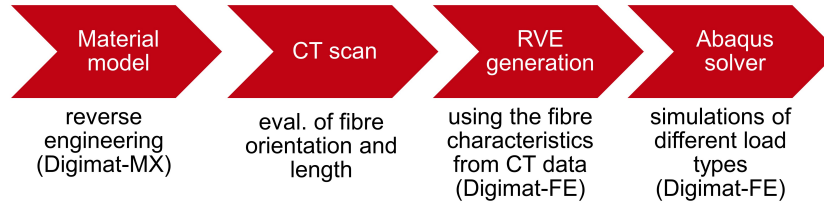
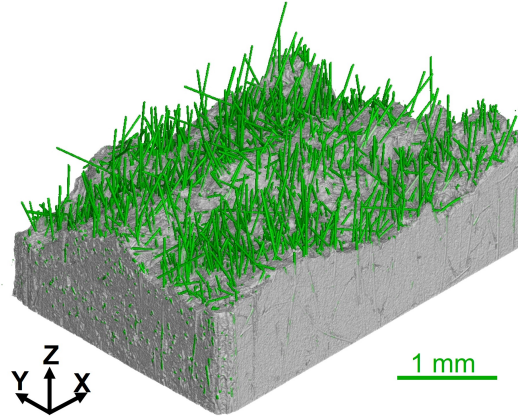FIGURE 2. Schematical workflow for the micro-mechanical simulations.

FIGURE 3. 3D rendered CT volume view of fracture surface with colored protruding fibres.

the Young's modulus, the Poisson's ratio, the yield stress, several hardening parameters and the aspect ratio until the model match the experimental results. Based on the fibre characterization data gained by CT, the RVE for the CR 0° test specimen was generated in Digimat-FE. A cubic RVE with a edge length of $500\,\mu$m was generated and filled with fibres of sphero-cylindrical shape. The nominal fibre content was set to $24\,\text{wt}\%$, the diameter was set to $13\,\mu$m and based on the fibre characterization by CT data a mean fibre length of around $470\,\mu$m was used. These characterization additionally provided the information on the fibre orientation distribution. An average fibre orientation tensor with a main orientation in z-direction was applied. The fibres were assumed to be perfectly bonded in the matrix with no failure criteria. The mechanical loading was selected with a periodic boundary condition and quasi-static mode. Finally, the micro structural simulations were performed with the abaqus solver for different load types.

3. Results and discussion

Due to a non-uniform stress distribution inside the materials, only fibres in direction of the force were considered for the estimation of the critical fibre length. Similar to other studies [8] [14], the estimation was performed based on the critical length model first reported by Fu et al. [15]. Assuming, that the fibre was pulled out of the other part by the same extent, the critical length can be estimated by selecting the longest pulled out fibre $l_{p,max}$ according Equation (2).

$$l_c \geq 2 * l_{p,max}, \tag{2}$$

In Figure 3 a 3D rendered view of the fractures surface and the segmented protruded fibres (coloured green) is shown.

Based on this data set, the ten longest fibres oriented in direction of the force were selected (fibre orientation tensor component $a_{ZZ} > 0.9$) and a mean value for the longest pulled out fibre length $l_{p,max}$ was calculated to get rid of any segmentation errors. According to 2 this resulted in a critical fibre length of around $1\,070\,\mu$m. Based on the Kelly-Tyson model and assuming a fibre strength of approximately $2\,500\,\text{MPa}$ as well as a nominal fibre diameter of $13\,\mu$m, the interfacial shear strength was calculated at around $15\,\text{MPa}$.

Figure 4a shows a comparison of the stress-strain curves of the monotonic tested, the interrupted tested and the simulated CR 0° test specimen. The lower stress values of the interrupted tested specimen can be explained by relaxation due to the longer testing procedure. Generally, deviations between experiments and simulations can be expected, especially in the plastic region, because of the used elastic-plastic material model and the assumed perfectly bonded fibres, which is indeed not the case. Nevertheless, the probability distribution of the maximum principal strains inside the material (normalized bins) show good accordance for simulation (approx. $740\,000$ nodes) and interrupted in situ experiment (approx. $3\,600$ nodes).

From the results of the micro structural simulation, two fibres were selected and the according strain distri-
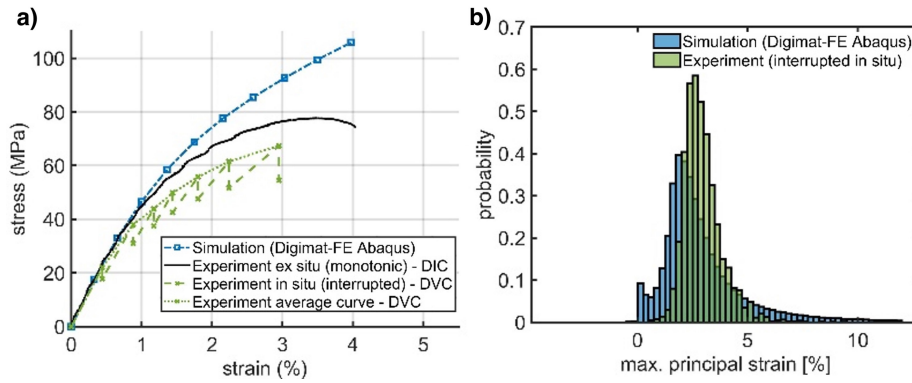
FIGURE 4. Stress-strain curves (a) and probability distribution of the maximum prinicipal strain (b) of experiments and simulation for the CR 0° test specimen [12].
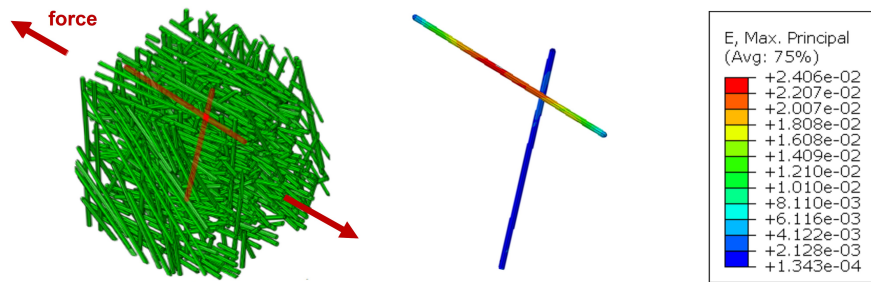

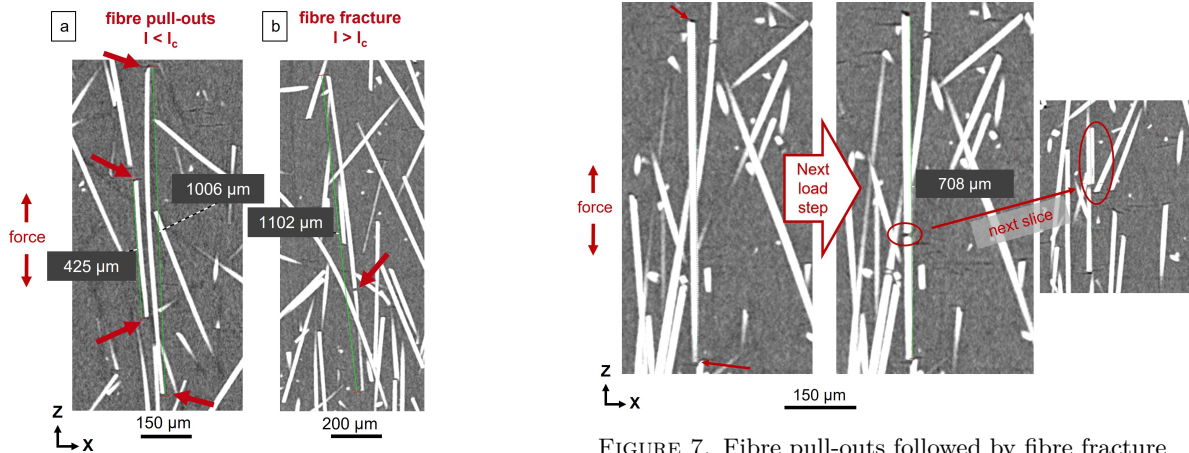FIGURE 5. RVE with selected fibres and strain distribution along these fibres. [13]

FIGURE 6. Sectional images of fibre pull-outs (a) and fibre fractures (b) with dimensions of selected fibres (green lines) and marked defects (red arrows).

FIGURE 7. Fibre pull-outs followed by fibre fracture ($l < l_c$).

bution along those single fibres were evaluated (shown in Figure 5).

The RVE simulation enabled the investigation of the strain along selected fibres. As expected the highest strain could be observed for fibres in direction of applied force, with a peak in the centre of the fibre, as theory reported. Therefore, fibre fracture is expected if the fibre length is longer than the critical length. For fibres oriented perpendicular to the applied force, the strain is significantly smaller.

In a next step, some comparable fibres were selected from the real structure. By using CT slice images of

the last volume data set before fracture, it was possible to measure the fibres. To achieve the maximum stress in the fibre, the fibre length must be greater than the critical length l_c. In Figure 6a two fibres, that are smaller than the critical length, are presented. According to theory, fibre pull out and no fibre fracture is expected, as the maximum stress in the fibre is not reached. The sectional image in Figure 6b shows a fibre which is slightly longer than the estimated critical fibre length of $1070\,\mu m$ and therefore fibre fracture can be observed.

Nevertheless, not all fibres smaller than the critical length pull-out. Some of them also fracture in a previous load step (see Figure 7). When scrolling
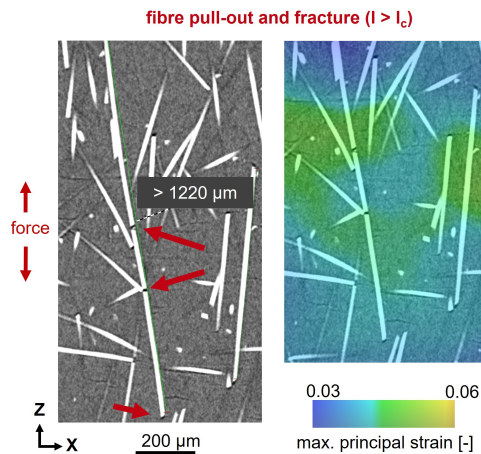
fibre pull-out and fracture (l > l_c)

Figure 8. Selected fibres showing fibre pull-outs and fibre fractures dependent on their length and neigbouring fibres(with overlayed max. principal strain distribution).
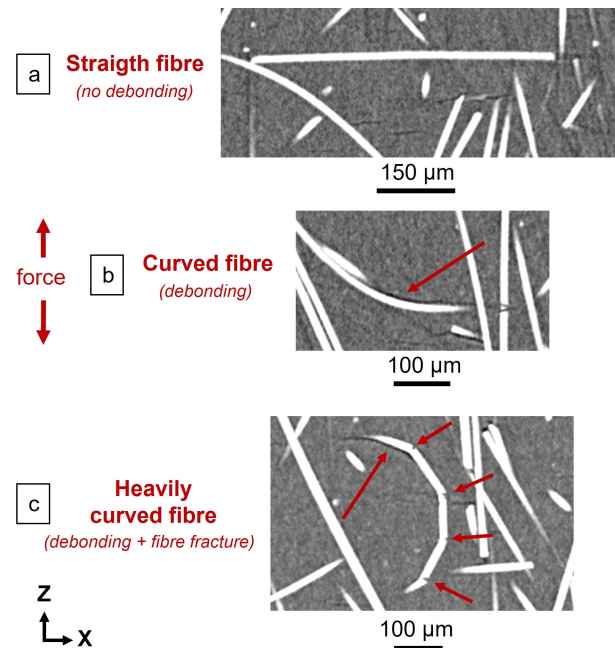

Figure 9. Further examples for different fibre curvatures, revealing no fibre/matrix failure (a), fibre-matrix debonding (b) and fibre fractures (c).

through the CT data, it can be recognized, that the reason for this behaviour might be neighbouring fibres, influencing the local stress and strain behaviour and thus leading to fibre fracture.

An further example is presented in Figure 8, where the fibre is longer than the critical fibre length. In this example the fibre fractured at two positions. Additionally, the strain distribution (correlating unloaded state with last load step before fracture) is shown. Figure 8 reveals that these two fracture positions are exactly at areas where there are a lot of neighbouring fibre ends, thus influencing the local strain distribution.

Further, other defect types can be found in the tested samples, for example matrix fracture and fibre matrix debonding. Some examples for the latter are presented in Figure 9. There is no load transmission to the fibre by shear for fibres aligned perpendicular to the force. Such cases can be treated as an interface crack between two dissimilar materials and thus might be to small to be quantified by CT. Another reason, why no greater fibre-matrix debonding defect is revealed, are probably surrounding defects like matrix fractures absorbing the load (Figure 9a). For curved fibres, the direction of load transmission changes (also due to neighbouring fibres) and again shear forces cause a fibre-matrix debonding (Figure 9b). Furthermore, heavily curved fibres could be identified, showing a lot of fibre fractures already in unloaded state and fibre-matrix debonding with increasing load (Figure 9c). Those defects are process induced and are critical with respect to their crack propagation potential.

4. Conclusions

Simulation results of the strain distribution along selected fibres correspond with theory and the expected fibre fracture behaviour. Nevertheless, the in situ experiments and a detailed look on various sectional images revealed that the fracture behaviour of individual fibres is strongly influenced by neighbouring fibres and the local strain distribution.

The determination of the fibre length of the ten longest free fibres oriented in direction of the applied force, allows for the approximation of the critical fibre length and the interfacial shear strength, based on the Kelly-Tyson model. However, this method and the obtained values are not verified by other methods so far. Further investigations should consider the influence of testing manner and sample geometry.

List of symbols

l_c critical fibre length [μm]

$l_{p,max}$ determined longest free fibre length (mean) [μm]

d fibre diameter [μm]

σ_{fibre} fibre strength [MPa]

τ_{fibre} interfacial shear strength [MPa]

References

[1] J. Kastner, C. Heinzl. X-ray tomography. In I. Nathan, N. Meyendorf (eds.), *Handbook of Advanced Non-Destructive Evaluation*, pp. 1095–1166. Springer, 2019.

[2] J. Maurer, M. Jerabek, D. Salaberger, et al. Stress relaxation behaviour of glass fibre reinforced thermoplastic composites and its application to the design of interrupted in situ tensile tests for investigations by X-ray computed tomography. *Polymer Testing* **109**:107551, 2022. `https://doi.org/10.1016/j.polymertesting.2022.107551`

[3] J. Maurer, D. Salaberger, M. Jerabek, et al. Quantitative investigation of local strain and defect formation in short glass fibre reinforced polymers using X-ray computed tomography. *Nondestructive testing*

and Evaluation **37**(5):582–600, 2022.
https://doi.org/10.1080/10589759.2022.2075865

[4] B. K. Bay, T. S. Smith, D. P. Fyhrie, M. Saad. Digital Volume Correlation: Three-dimensional strain mapping using X-ray tomography. *Experimental Mechanics* **39**(3):217–226, 1999.
https://doi.org/10.1007/bf02323555

[5] A. Vrgoč, Z. Tomičević, B. Smaniotto, F. Hild. Characterization of glass fiber reinforced polymer via Digital Volume Correlation: Investigation of notch sensitivity. *Mechanics of Materials* **177**:104552, 2023.
https://doi.org/10.1016/j.mechmat.2022.104552

[6] J. Holmes, S. Sommacal, Z. Stachurski, et al. Digital image and volume correlation with X-ray micro-computed tomography for deformation and damage characterisation of woven fibre-reinforced composites. *Composite Structures* **279**:114775, 2022. https://doi.org/10.1016/j.compstruct.2021.114775

[7] E. Schöberl, C. Breite, A. Melnikov, et al. Fibre-direction strain measurement in a composite ply under quasi-static tensile loading using Digital Volume Correlation and *in situ* Synchrotron Radiation Computed Tomography. *Composites Part A: Applied Science and Manufacturing* **137**:105935, 2020. https://doi.org/10.1016/j.compositesa.2020.105935

[8] L. Vas, F. Ronkay, T. Czigány. Active fiber length distribution and its application to determine the critical fiber length. *Polymer Testing* **28**(7):752–759, 2009.
https://doi.org/10.1016/j.polymertesting.2009.06.006

[9] A. Kelly, W. Tyson. Tensile properties of fibre-reinforced metals: Copper/tungsten and copper/molybdenum. *Journal of the Mechanics and Physics of Solids* **13**(6):329–350, 1965.
https://doi.org/10.1016/0022-5096(65)90035-9

[10] D. Salaberger. *Micro-structure of discontinuous fibre polymer matrix composites determined by X-ray Computed Tomography.* Ph.D. thesis, 2019.
https://doi.org/10.34726/hss.2019.64362

[11] B. Fröhler, J. Weissenböck, M. Schiwarth, et al. open_iA: A tool for processing and visual analysis of industrial computed tomography datasets. *Journal of Open Source Software* **4**(35):1185, 2019.
https://doi.org/10.21105/joss.01185

[12] J. Maurer, D. Krölling, M. Jerabek, et al. Local stress-strain behaviour in short glass fibre reinforced polymers - a comparison of different simulation approaches with experimental results based on X-ray computed tomography data. *Proceedings of the 20th European Conference on Composite Materials, Composites Meet Sustainability, Vol 1 - Materials, ECCM20 Lausanne, Switzerland* pp. 1160–1167, 2022. https://doi.org/10.5075/epfl-298799_978-2-9701614-0-0

[13] D. Krölling. *Investigation of a short-fibre reinforced polymer using micro-computed tomography and micro-mechanical simulations.* Master's thesis, 2022.

[14] D. Salaberger, M. Jerabek, W. Stockreiter. Estimation of interfacial shear strength of long glass fibre composites by X-ray computed tomography. *Composites Meet Sustainability - Proceedings of the 20th European Conference on Composite Materials, ECCM20 Lausanne, Switzerland* pp. 1146–1151, 2022. https://doi.org/10.5075/epfl-298799_978-2-9701614-0-0

[15] S. Fu, B. Lauke, Y. Zhang, Y.-W. Mai. On the post-mortem fracture surface morphology of short fiber reinforced thermoplastics. *Composites: Part A* **36**(7):987–994, 2005. https://doi.org/10.1016/j.compositesa.2004.11.005